Electronic Supplementary Material (ESI) for Journal of Materials Chemistry C.
This journal is © The Royal Society of Chemistry 2022

[Supporting Information]

Anion Chemical Composition of Poly(ethylene oxide)-based Ionomers Controls Ion Aggregation and Conduction

Wenwen Mei[1], Deyang Yu[2], Christy George[3], Louis A. Madsen[2], Robert J. Hickey[1,4,*], Ralph H. Colby[1,4,*]

[1]Materials Science and Engineering, The Penn State University, University Park, PA16802, USA

[2]Department of Chemistry and Macromolecules Innovation Institute, Virginia Tech, Blacksburg, VA 24061

[3]Department of Chemistry, The Penn State University, University Park, PA16802, USA

4Materials Research Institute, The Penn State University, University Park, PA16802, USA

*Corresponding Authors: rjh64@psu.edu and rhc5@psu.edu

Contents

I. Characterization of Single-ion Conductors with SEC and ^{1}H NMR

Ionomers MTLi and MSLi with different ion content were synthesized with reversible addition-fragmentation chain transfer polymerization (RAFT). The RAFT agent, 4-cyano-4-(phenylcarbonothioylthio)pentanoic acid, was specifically chosen due to preferable polymerization kinetics using methacrylate monomers. The molecular weights of the synthesized ionomers were characterized using size-exclusion chromatography (SEC) with a 0.05 M LiBr/DMF solution as the mobile phase. The SEC traces are plotted in **Figure S1**. Poly(ethylene glycol) (PEG) standards were used for M_n calibration. Reported M_n values for synthesized ionomers are listed in **Table 1**.

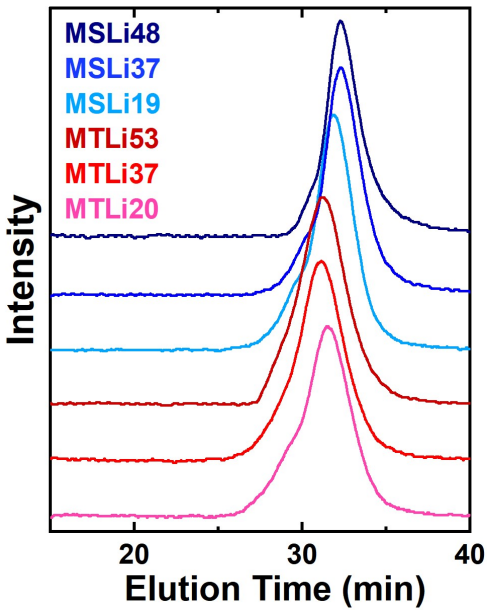

Figure S1. SEC traces for the synthesized MSLi and MTLi ionomers. SEC measurements were conducted at 40 °C using a RI detector with a 0.05 M LiBr/DMF solution as the mobile phase.

^{1}H NMR was used to identify the copolymer composition for (MSLi19) and (MTLi20) (**Figures S2** and **S3**). The copolymer composition was determined by integrating the ^{1}H NMR spectra.

Specifically, the ionic composition of MSLi19 is determined to be $\frac{0.39/2}{2/2} = 0.19$, and the ionic composition of MTLi20 is determined to be $\frac{2.21 - 2 * 3.14/3}{2/2} = 0.20$.

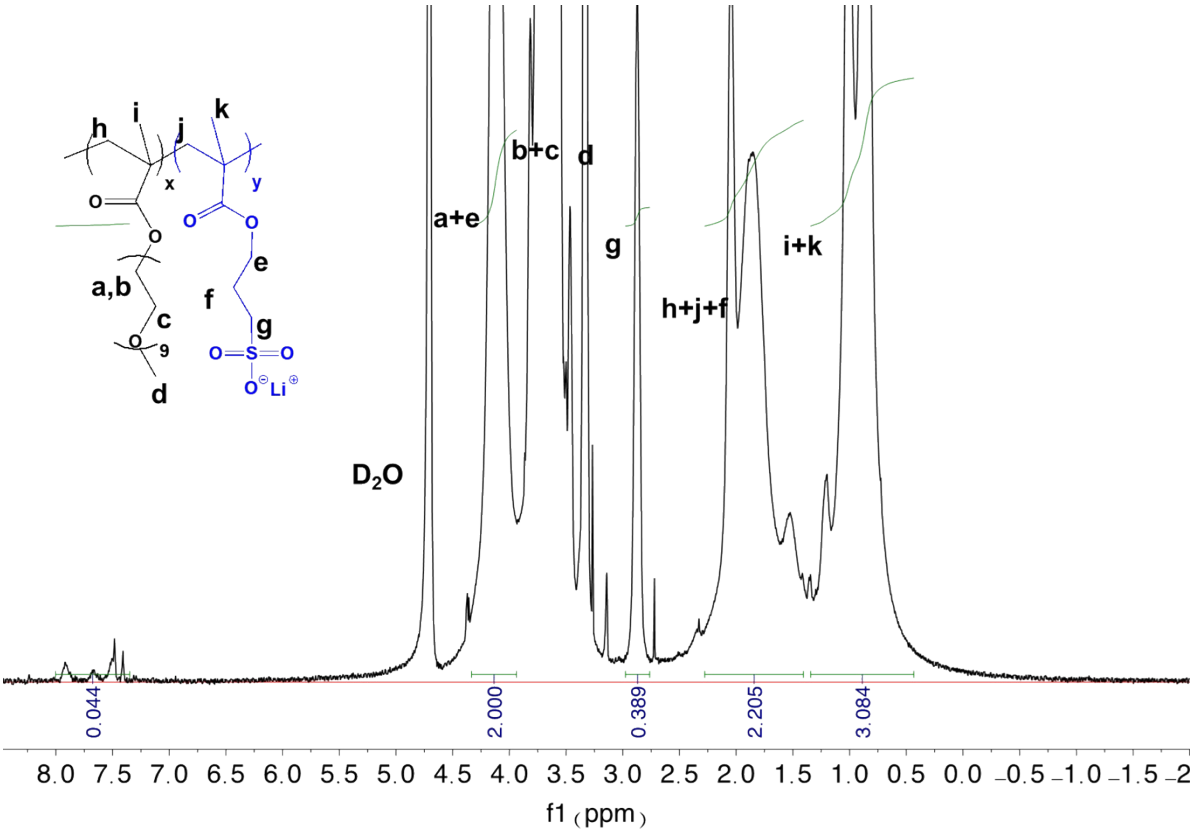

Figure S2. ^{1}H NMR spectrum for MSLi19 in deuterated water (D_2O) recorded at 400 MHz. Note that "a" represents COOCH2- and "b" represents -OCH2CH2- of the PEO9 repeat unit.

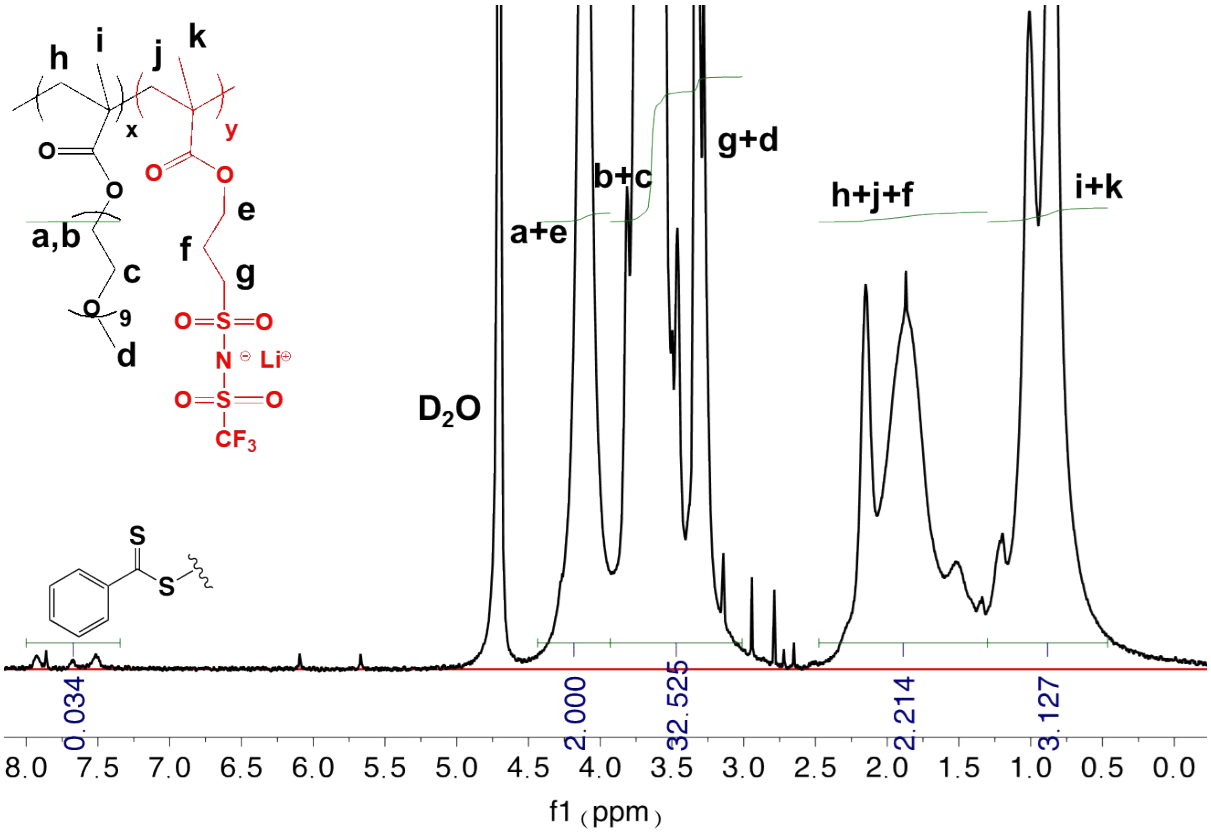

Figure S3. ^{1}H NMR spectrum for MTLi20 in D_2O recorded at 400 MHz. Note that "a" represents COOCH2- and "b" represents -OCH2CH2- of the PEO9 repeat unit.

Additionally, end group analysis was performed for the synthesized ionomers to yield the M_n and degree of polymerization (N). The integration at 7.3−8.0 ppm is from the RAFT agent, and the end group analysis suggests that the degree of polymerization for the MTLi20 and MSLi19 are:

$$X_n = \frac{2/2}{0.044/5} = 114$$

The M_n estimated based on the end group analysis with known copolymer composition determined from ^{1}H NMR is 54.4 kg/mol for MSLi19 and 57.4 kg/mol for MTLi20. The estimated M_n for synthesized single-ion conductors are listed in **Table 1**.

Figure S4a compares the composition of the monomer feed with the composition of the final copolymer. The composition of the synthesized copolymer is very close to the composition of the monomer feed with different monomer feeds (~ 80% conversion) (**Figure S4a**). The polymerization was also monitored via ^{1}H NMR under differerent conversions by taking aliquots at different reaction times. The aliquots are first characterized with ^{1}H NMR to determine the conversion and then dialyzed to remove the unreacted monomers to identify the resultant copolymer composition, showing similar monomer and copolymer compositions (**Figure 1**).

The copolymer composition is close to the monomer feed with different conversions and monomer feeds, confirming that the synthesized ionomers are random with minimal compositional drift. We further estimated the reactivity ratio based on the linearized Lewis-Mayo equation using data from **Figure S4a** shown in **Figure S4b**,[1, 2] giving reactivity ratios of 0.81 for MSK and 0.80 for PEO9

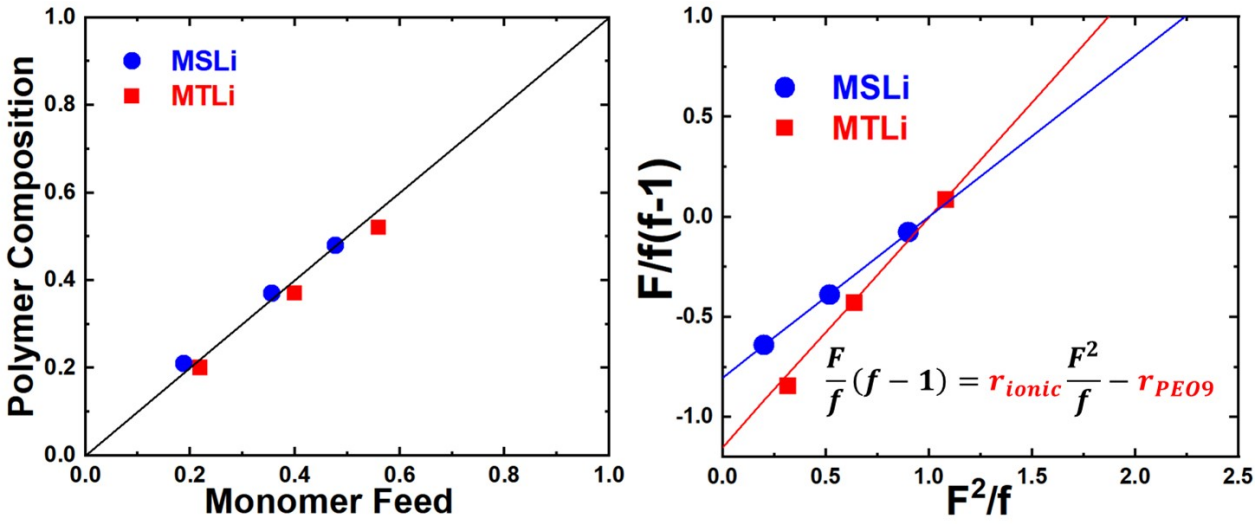

of the MSLi ionomers, and 1.1 for MTLi and 1.1 for PEO9 for the MTLi ionomers.

Figure S4. (a) Comparing the polymer composition with monomer feed based on the molar fraction of ionic monomers (~ 80% conversion). (b) Plotting the linearized Lewis-Mayo equation

for MSK and MTLi. F is the molar monomer composition (ionic/PEO9) and f is the molar polymer composition (ionic/PEO9).

II. Glass Transition Temperature Characterized from Differential Scanning Calorimetry (DSC) and Dielectric Relaxation Spectroscopy (DRS).

The glass transition temperature (T_g) was measured using DSC. **Figure S5** shows the second heating trace with a heating and cooling rates of 20 K/min. T_g is defined as the midpoint of heat capacity change and is indicated with the arrow. An evident broadening of the glass transition temperature range is observed for ionomers with higher ion content because of the increased structural heterogeneity. The T_g increases significantly for MTLi with higher ion content because of the increased number density of solvated sulfonylimide ion pairs (see X-ray results shown in **Figure 3**). In contrast, the measured T_g for MSLi is relatively insensitive to ion content since MSLi aggregates most of the ions, so there are very few sulfonate lithium ion pairs in the PEO matrix.

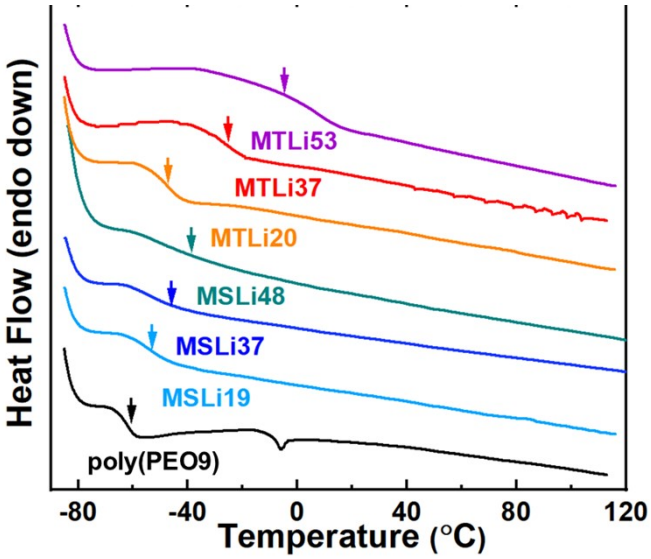

Figure S5. DSC traces for synthesized ionomers taken from the second heating under a heating/cooling rate of 20 K/min. Arrows indicate T_g determined from the midpoint of the heat capacity change. Data for poly(PEO9) are included for comparison.

The DSC T_g represents the low-T_g phase for MSLi, which is further supported by the DRS measurements. The dielectric spectra are shown in **Figure S6a** for MSLi19 at 303 K, indicating one broad relaxation process α. The temperature dependence of the α process is fitted with the VFT equation Eq. S1 (**Table S1** lists the fitting parameters),[3] and gives the DRS T_g (where $\omega_\alpha(T)$ is extrapolated to $\omega_\alpha(T_g) = 0.01\ rad/s$) in good agreement with the measured DSC T_g. (**Table S1** and **Figure 7**).

$$\omega_\alpha(T) = \omega_\infty exp(-\frac{DT_0}{T - T_0}) \qquad \text{Eq. S1}$$

Because most sulfonate-lithium ion pairs form in aggregates, the few solvated ion pairs in the PEO matrix show a minimal relaxation strength (hence small ε_s) due to the small number density of solvated sulfonate lithium ion pairs and also an insignificant change of measured T_g (from both DSC and DRS) with increasing ion content. The derivative spectra $\varepsilon_{der}(\omega) = -\frac{\pi \partial \varepsilon'(\omega)}{2\ \partial ln\omega}$ (open blue squares) of MSLi19 are fitted with Eq. S2 with one Havriliak-Negami (HN) term that accounts for the α processes.[4-6]

$$\varepsilon'(\omega) = \frac{\Delta\varepsilon_\alpha}{(1 + (\frac{i\omega}{\omega_{HN,\alpha}})^\alpha)^b} + A\omega^{-n} + \varepsilon_\infty \qquad \text{Eq. S2}$$

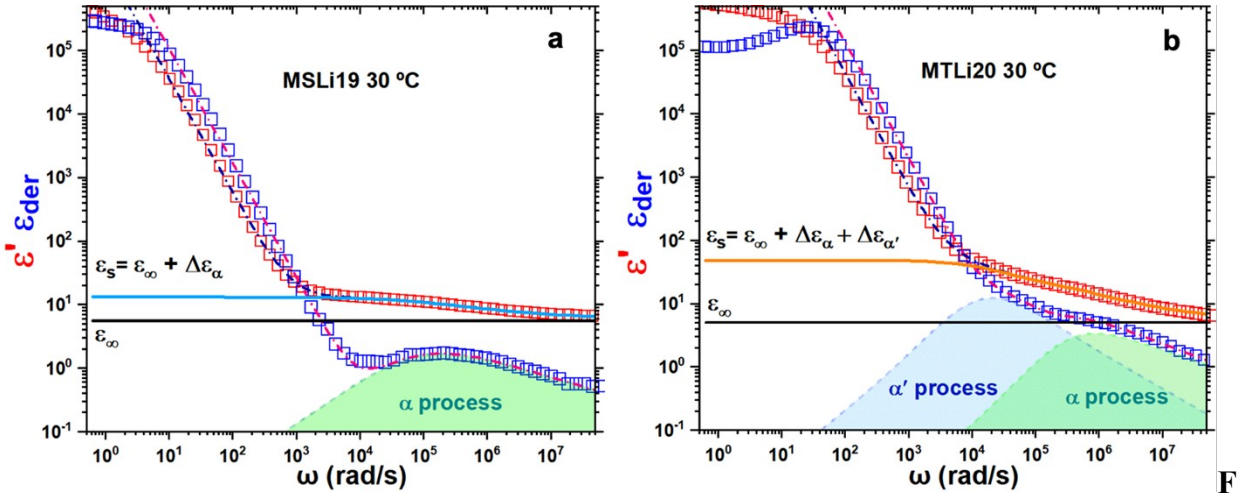

Figure S6. Dielectric spectra for (a) MSLi19 and (b) MTLi20 at 303 K measured with sandwich cells (top electrode diameter = 10mm, bottom electrode diameter = 30mm, sample thickness = 0.1 mm). Open symbols are data from DRS measurements and dashed lines are fittings based on Eq. S2 and Eq. S3 with n = 1.82 and ε_∞ = 5.5 for MSLi19 and 4.5 for MTLi (see **Table S2** for fitting parameters).

Figure S6b shows the dielectric spectra for MTLi20 at 303 K, where two relaxation processes α and α′ are identified. The much better solvated sulfonylimide lithium ion pairs give rise to a substantial dielectric relaxation strength and consequently much larger ε_s. Similarly, the DRS spectra are fitted based on Eq. S3 with two Havriliak-Negami (HN) terms that account for the α and α′ processes.[4, 5, 7]

$$\varepsilon'(\omega) = \frac{\Delta\varepsilon_\alpha}{(1+(\frac{i\omega}{\omega_{HN,\alpha}})^a)^b} + \frac{\Delta\varepsilon_{\alpha'}}{(1+(\frac{i\omega}{\omega_{HN,\alpha'}})^{a'})^{b'}} + A\omega^{-n} + \varepsilon_\infty \qquad \text{Eq. S3}$$

The second term is a power law description of electrode polarization with exponent n = 1.82.

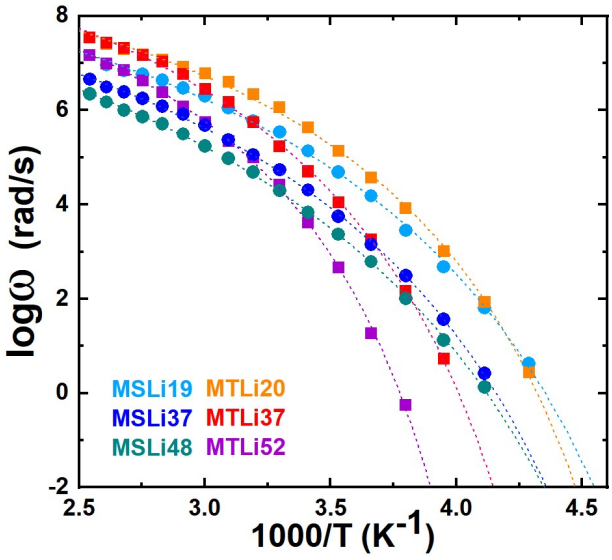

Figure S7. Temperature dependence of ω_α and the corresponding VFT fitting based on Eq. S1.

Table S1. VFT fitting parameters of Eq. S1 in the main text for the α-relaxation and comparison of DRS T_g and DSC T_g for the six ionomers.

Ionomer	***D***	T_0 **(K)**	**log(ω_∞) (rad/s)**	$T_{g,DRS}$ **(K)**	$T_{g,DSC}$ **(K)**
MSLi19	7.54	172	9.72	226	218
MSLi37	7.91	177	9.49	229	225
MSLi48	9.35	170	9.43	232	229
MTLi20	6.04	183	10.0	224	223
MTLi37	6.35	197	10.4	241	244
MTLi52	5.50	223	10.2	267	271

Table S2. Fitting parameters for derivative spectra with Eq. S2 and Eq. S3.

	a	**b**	**a'**	**b'**	**n**	ε_∞
MTLi20	0.8	0.41	0.78	0.73	1.82	4.5

MTLi38	0.8	0.41	0.78	0.73	1.82	4.5
MTLi52	0.8	0.41	0.78	0.73	1.82	4.6
MSLi19	0.64	0.47	NA	NA	1.82	5.5
MSLi37	0.7	0.45	NA	NA	1.82	5.5
MSLi48	0.76	0.47	NA	NA	1.82	5

III. ^{7}Li NMR Measurements.

The T_1 relaxation time for MTLi decreases with increasing temperature. It suggests the system is in the spin diffusion limit (i.e., the low-temperature flank where T_1 shows a minimum in temperature dependence). **Table S3** lists the measured T_1 values at 150 °C and 80 °C for the investigated ionomers.

Table S3. Lithium ion T_1 (in seconds) at 150 °C and 80 °C.

^{7}Li T_1 (s)	**MTLi 20**	**MTLi 37**	**MTLi 53**	**MSLi 19**	**MSLi 38**	**MSLi 48**
150 °C	0.71	0.67	0.65	0.66	1.5	2.0
80 °C	0.52	0.56	0.89	1.1	2.2	2.6

Figure S8 demonstrates the 1D ^{7}Li NMR spectra of the investigated ionomers at 80 °C. The peak width is broader than the peak width measured at 150 °C for the same sample (**Figure 6**). Furthermore, an apparent broadening of the peak width is observed with increasing ion content due to the enhanced interaction between Li^{+}. As discussed in the main text, the considerably broader peak for MSLi compared with MTLi is consistent with severe ion aggregation in MSLi.

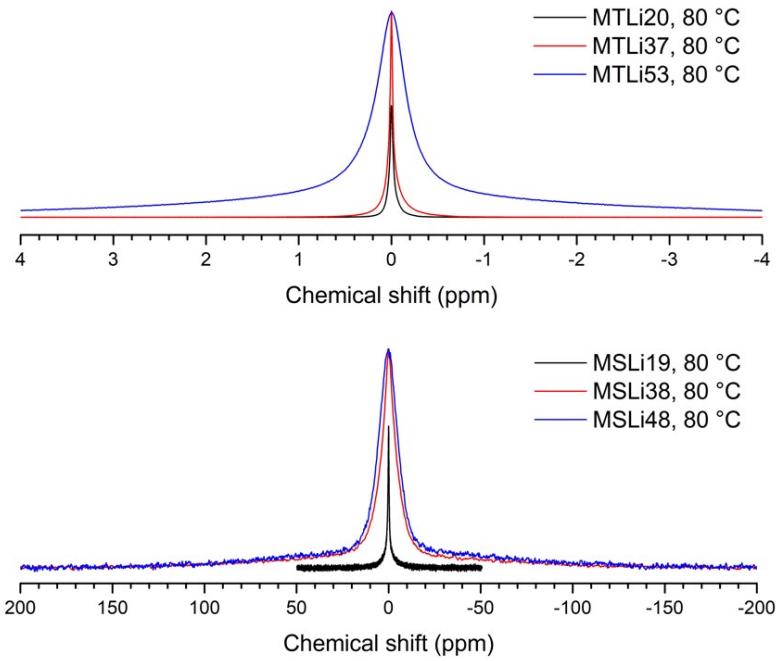

Figure S8. 1D ^{7}Li NMR spectrum of the single-ion conducting ionomers at 80 °C. The radio frequency (RF) pulse length was set to 5 μs for MSLi38 and MSLi48, and a 90 ° pulse length (19 μs) was used for all other samples.

Figure S9 compares full width at half maximum (FWHM) for the 1D ^{7}Li NMR spectra of the investigated ionomers at 80 °C (open symbols) and 150 °C (filled symbols). The peak width is broader at 80 °C than at 150 °C. Raising ion content results in larger FWHM values due to the increased heterogeneity of the local Li^{+} environment. Significant ion aggregation for MSLi results in a much broader peak than MTLi.

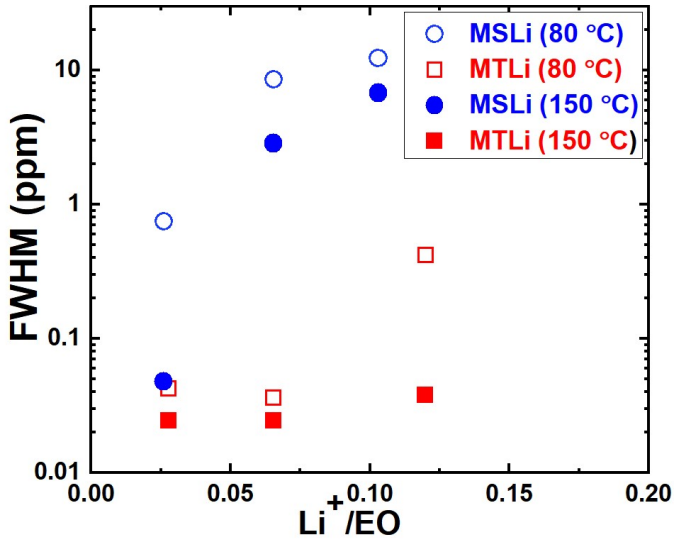

Figure S9. Full width at half maximum (FWHM) for the 1D ^{7}Li NMR spectra of the investigated ionomers at 80 °C (open symbols) and 150 °C (filled symbols).

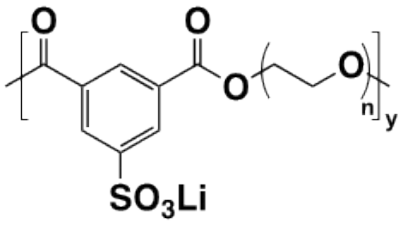

Figure S10. Chemical structure of PEO9-100Li, PEO13-100Li and PEO24-100Li compared in **Figure 5,6**.[8, 9]

IV. Comparing Sulfonate Anion and Sulfonylimide Anion Based on DFT Calculations.

Here, a simple calculation based on Tomasi's solvation model is used to calculate the enthalpic gain of forming an ion pair and a quadrupole (representing aggregates) from neat Li^+ and anion:[10, 11]

$$\Delta E_{pair} = E_{Li+} + E_{anion} - E_{pair}$$

$$\Delta E_{quad} = 2E_{Li+} + 2E_{anion} - E_{quad}$$

The calculation is based on a basis set of 6-31++G(d,p) with a PCPM solvation model (diethyl ether) using Gaussian09 software. The ratio between $^{\Delta E_{quad}}$ and $2*^{\Delta E_{pair}}$ indicates whether the ion pair state or the quadrupole state (aggregation state) is more stable, inferring aggregation tendency based on anion chemistry. **Table S4** lists the calculated values for the sulfonate lithium-ion and sulfonylimide lithium-ion pairs. The results suggest that forming quadrupoles is more favorable for the sulfonate anion than the sulfonylimide anion, indicated by the higher $^{\Delta E_{quad}}$ and the quadrupole factor[13] $^{\Delta E_{quad}}/_{2 * \Delta E_{pair}}$. The molecular output configurations are shown in **Figure S11**.

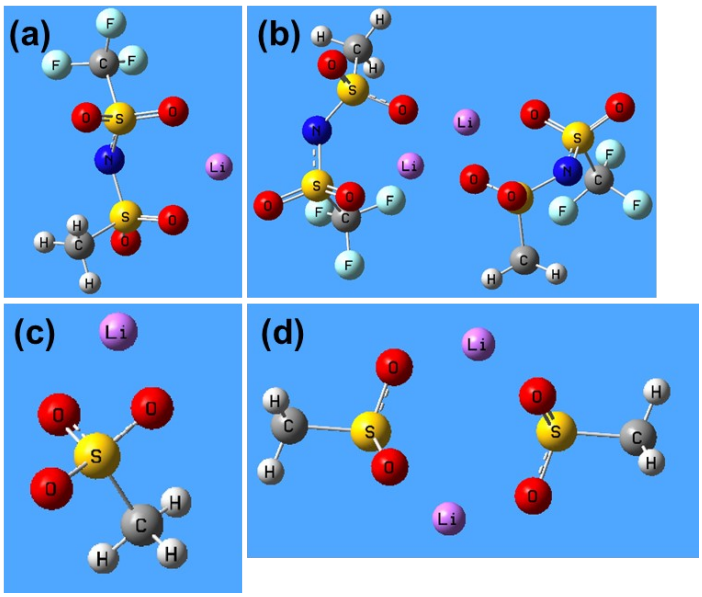

Figure S11. Molecular output geometry based on a basis set of 6-31++G(d,p) with a PCPM solvation model (diethyl ether) for sulfonylimide-lithium pair (a), for sulfonylimide-lithium quadrupole (b), sulfonate-lithium pair (c) and sulfonate-lithium quadrupole (d).

Table S4. Energy difference to form a pair and a quadrupole from neat Li^+ and neat anion.

	ΔE_{pair} (kJ/mol)	ΔE_{qua} (kJ/mol)	$\Delta E_{qua}/2 * \Delta E_{pair}$
CH_3SO_3Li	170	417	1.23
$CH_3SO_2NSO_2CF_3$	161	369	1.14

Li^+ favorably interacts with the oxygen from anions and the ethylene oxide units from PEO9,[12, 13] which allows us to further compare the Mulliken charge for the oxygen atoms from the sulfonate and sulfonylimide anion and dimethyl ether (which represents the ethylene oxide units from PEO9) based on PCPM (solvent=diethyl ether). The values for oxygen atoms are listed in **Table S5**. The oxygen atom is most negative in sulfonate and least negative in dimethyl ether and indicates the negative charge is more localized in the sulfonate anion than the sulfonylimide anion.

Table S5. Mulliken charges for O atoms from sulfonate, sulfonylimide, and dimethyl ether.

	Mulliken charge from oxygen atoms
CH_3SO_3Li	-0.68, -0.68, -0.66
$CH_3SO_2NSO_2CF_3$	-0.56, -0.57, -0.57, -0.55
CH_3OCH_3	-0.38

The DFT calculations indicate that the sulfonate anion is more charge localized (more negative Mulliken charge for oxygen atom) than the delocalized sulfonylimide anion. The Li^+ cation prefers to form quadrupoles (and presumably other larger aggregates) instead of isolated ion pairs (higher ΔE_{quad} and $\Delta E_{quad}/2 * \Delta E_{pair}$) with sulfonate anions. In contrast, the formation of quadrupoles with sulfonylimide is less favorable (smaller ΔE_{quad} and $\Delta E_{quad}/2 * \Delta E_{pair}$) which means that MTLi is

expected to have more isolated ion pairs than MSLi, consistent with both X-ray scattering and DSC results.

References

1. F. R. Mayo and F. M. Lewis, *J. Am. Chem. Soc.*, 1944, **66**, 1594-1601.
2. M. Fineman and S. D. Ross, *J. Polym. Sci.*, 1950, **5**, 259-262.
3. H. Vogel, *Phys. Z*, 1921, **22**, 645-646.
4. S. Havriliak and S. Negami, *J. Polym. Sci. Polym. Symp.*, 1966, **14**, 99-117.
5. A. Schönhals and F. Kremer, in *Broadband Dielectric Spectroscopy*, eds. F. Kremer and A. Schönhals, Springer Berlin Heidelberg, Berlin, Heidelberg, 2003, DOI: 10.1007/978-3-642-56120-7_3, pp. 59-98.
6. D. Fragiadakis, S. Dou, R. H. Colby and J. Runt, *J. Chem. Phys.*, 2009, **130**, 064907.
7. U. H. Choi, A. Mittal, T. L. Price, H. W. Gibson, J. Runt and R. H. Colby, *Macromolecules*, 2013, **46**, 1175-1186.
8. N. H. LaFemina, Q. Chen, R. H. Colby and K. T. Mueller, *J. Chem. Phys.*, 2016, **145**, 114903.
9. S. Dou, S. Zhang, R. J. Klein, J. Runt and R. H. Colby, *Chem. Mater.*, 2006, **18**, 4288-4295.
10. J. Tomasi and M. Persico, *Chem. Rev.*, 1994, **94**, 2027-2094.
11. H.-S. Shiau, W. Liu, R. H. Colby and M. J. Janik, *J. Chem. Phys.*, 2013, **139**, 204905.
12. A. G. Baboul, P. C. Redfern, A. Sutjianto and L. A. Curtiss, *J. Am. Chem. Soc.*, 1999, **121**, 7220-7227.
13. R. L. Jarek, T. D. Miles, M. L. Trester, S. C. Denson and S. K. Shin, *The Journal of Physical Chemistry A*, 2000, **104**, 2230-2237.